

Gertsenshtein-Zel'dovich effect explains the origin of Fast Radio Bursts

Ashu Kushwaha,^{1,*} Sunil Malik^{b,1,2,3,‡} and S. Shankaranarayanan^{1,§}

¹*Department of Physics, Indian Institute of Technology Bombay, Mumbai 400076, India*

²*Institut für Physik und Astronomie, Universität Potsdam,*

Haus 28, Karl-Liebknecht-Str. 24/25, D-14476 Potsdam, Germany

³*Deutsches Elektronen-Synchrotron DESY,*

Platanenallee 6, D-15738 Zeuthen, Germany

Abstract

We present a novel model that explains the origin of Fast Radio Bursts (FRBs) — short (< 1 s), bright (0.1 – 1000 Jy) bursts of GHz frequency radio waves. The model has three ingredients — compact object, progenitor with effective magnetic field strength around 10^{10} Gauss, and GHz frequency gravitational waves (GWs). The energy conversion from GWs to electromagnetic waves occurs when GWs pass through the magnetosphere of such compact objects due to the Gertsenshtein-Zel'dovich effect. This conversion produces bursts of electromagnetic waves in the GHz range, leading to FRBs. Our model has three key features: (i) can generate peak-flux up to 1000 Jy, (ii) can naturally explain the pulse-width and (iii) predict FRB's random and repeating nature with a wide flux range. We thus conclude that the millisecond pulsars could be the progenitor of FRBs. Further, our model offers a novel perspective on the indirection detection of GWs at high-frequency beyond detection capabilities. Thus, transient events like FRBs are a rich source for the current era of multi-messenger astronomy.

^b Corresponding Author

* ashu712@iitb.ac.in

‡ sunil.malik@uni-potsdam.de

§ shanki@phy.iitb.ac.in

Technological advancement has fuelled research in high-energy astrophysical phenomena at larger redshift ranges, and we are in a position to address some unresolved questions starting from pulsar emission mechanism [1] to short bursts such as Gamma-ray bursts (GRBs) [2], Fast radio bursts (FRBs) [3–5]. To date, more than 600 FRBs have been reported in various catalogues [5–9]. 99% of these FRBs have the following two characteristic features: peak flux (S_ν) varies in the range $0.1 \text{ Jy} < S_\nu < 700 \text{ Jy}$ and the pulse width is less than a second [6, 9]. These observations have posed the following questions: What causes these extreme high-energy transient radio-bursts from distant galaxies, lasting only a few milliseconds each [3–5]? Why do some FRBs repeat at unpredictable intervals, but most do not [5]? Does strong gravity provide an active role?

This work addresses one of the open questions of FRBs, namely *the origin of the large amount of energy released in a short time* [3–9]. Since the time scale of these events is less than a second, the astrophysical processes that explain these events *cannot* be thermal [3]. Naturally, many models involving non-thermal processes such as Synchrotron radiation [10], black hole super-radiance [11], evaporating primordial black hole [12, 13], spark from cosmic strings [14], Quark Novae [15] have been proposed. Despite the use of exotic new physics, no single model has yet been able to provide a universal explanation for the enormous energy released in these events.

One key missing ingredient, as we show below, is the *dynamics of strong-gravity*. The Spatio-temporal changes in the strong-gravity regime — oscillons, phase transitions, plasma instability, primordial black holes, reheating — generate gravitational waves (GWs) in a broad range of frequencies ($10^{-15} - 10^{15} \text{ Hz}$) [16–21]. GWs carry an enormous amount of energy. A typical GWs from a compact binary collapse with amplitude $h \sim 10^{-22}$ carry the energy of the order of 10^{20} Jy [22, 23]. If the GWs indeed carry a lot of energy, can this energy transform into other observable forms of energy?

A physics maxim is that energy can be transformed between different forms. Although the total energy is conserved, the efficiency of the transformation depends on the energy scale, background dynamics, and external conditions (parameters). Energy transformation is one way to probe strong gravity regions like the early-universe, black-holes, and NS. In this work, we propose a novel approach that uses the energy conversion from GWs to electromagnetic (EM) waves that can *explain milli-second bursts like FRBs*. More specifically, GWs get converted to EM waves in the presence of strong transverse magnetic fields — Gertsenshtein-

Zel'dovich (GZ) effect [24–27]. To understand the GZ effect, let us consider GWs with a frequency ω_g passing through a region with high transverse static magnetic field \mathbf{B} . The propagation of GWs leads to compression and stretching of the magnetic field proportional to $h\mathbf{B}$ (h is the amplitude of GWs), which acts as a source leading to the generation of EM waves [24, 25]. The induced (resultant) EM waves generated will have maximum amplitude at resonance, i. e. frequency of EM waves is identical to ω_g . (For details, see appendix)

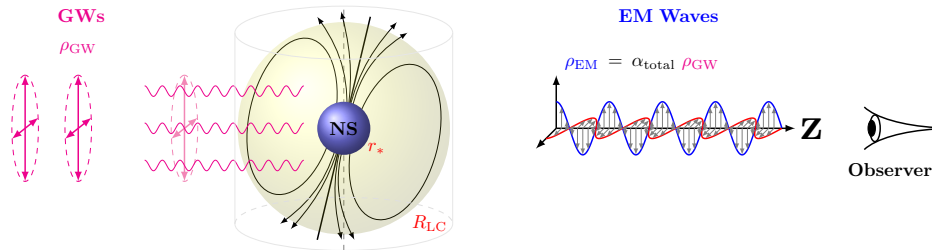


FIG. 1. Schematic depiction of Gertsenshtein-Zel'dovich effect showing the conversion of the GWs to the EM waves in the magnetosphere. The blue region corresponds to NS with radius r_* and the yellow region around NS corresponds to magnetosphere of radius R_{LC} . The black curves correspond to the magnetic field lines.

We show that the *GZ effect explains the origin of FRBs*. To explain the energy bursts in FRBs, we propose a model with the following two realistic assumptions: (i) the astrophysical object is compact and has a strong gravity environment, and (ii) the object possesses a small time-dependent magnetic field on the top of the large, effective static, transverse magnetic field. These two assumptions principally lead us to stellar remnants, such as NS and magnetars with magnetic field strength ranging from $10^8 - 10^{15}$ G [3, 4, 28, 29]. The small time-dependent magnetic fields arise due to the rotation of the NS about its axis with frequency ω_B [5, 29–32]. We consider ω_B in the range $[1, 10^3]$ Hz [10]. As a result, the effective magnetic field at a given point in the NS magnetosphere is $\mathbf{B}(t) = \mathbf{B}^{(0)} + \delta\mathbf{B} \sin(\omega_B t)$. It has been noted that $|\delta\mathbf{B}/\mathbf{B}^{(0)}|$ can be as large as 0.1 [32]. Here, we take $|\delta\mathbf{B}/\mathbf{B}^{(0)}| \sim 10^{-2}$.

Fig. 1 gives the schematic depiction of the physical model to explain the energy burst in FRBs. Consider GWs generated due to astrophysical processes [20, 22] passing through the magnetosphere of NS. In the figure, the magnetosphere is depicted as a cylinder. Due to the GZ effect, GWs are converted to EM waves as they pass through the magnetosphere [24, 25].

This conversion occurs at all points in the magnetosphere. Therefore, a faraway observer will see the integrated effect happening in the entire magnetosphere in this short duration. For example, light cylinder radius (R_{LC}) for a typical NS is $\sim 10^7 - 10^9$ cm, implying that the GWs take less than one second to cover the entire magnetosphere. This is one of the primary ingredients to support our analysis for the FRB observations.

To compute the GZ effect at a point in the magnetosphere, we consider Maxwell's equations on the background space-time with GW fluctuations. The linearized Einstein's equations, up to first order in the space-time perturbations are highly accurate. Note that in this approximation, the effects of GWs on the stress-tensor (Riemann tensor) are negligible. Hence, we consider background space-time to be Minkowski (in cartesian coordinates) [33?]). The two polarizations of GW (with frequency ω_g and wave-vector k_g) propagating along the z-direction are:

$$h_+ = A_+ e^{i(k_g z - \omega_g t)}, h_\times = iA_\times e^{i(k_g z - \omega_g t)}, \quad (1)$$

where A_+ and A_\times are the constant amplitudes of the GWs. We assume that both the modes of GWs are generated with an equal amount of energy, i.e., $|A_+| = |A_\times|$ — the isospectrality condition in general relativity [34].

As mentioned above, the key requirement of the GZ-effect is the presence of the transverse magnetic field in the direction of propagation of GWs. Besides, the time taken by the GWs to pass through the entire magnetosphere is much smaller than the rotation period of the millisecond pulsar/magnetar (ω_B^{-1}). Given the direction of propagation of GWs along the z-axis, the effective time-dependent transverse magnetic field is taken to be $\mathbf{B}(t) = (0, B_y^{(0)} + \delta B_y \sin(\omega_B t), 0)$ [31, 32].

Although the effective magnetic field will also depend on the distance from the surface of the object [3, 4, 28, 29], we assume that $\mathbf{B}(t)$ is independent of the distance from the surface up to R_{LC} [10]. Assuming that the NS magnetic field is dipolar, one can easily show that we can approximate the average magnetic field at any point in the magnetosphere to be constant. For completeness, details in the appendix.

Given the above setup, we now evaluate the GZ-effect in the magnetosphere of the NS and compare it with observational quantities in two steps:

1. First step involves evaluating the conversion from GWs to EM waves at a typical point inside the magnetosphere. This is referred to as *conversion factor* (α). We then obtain

the total conversion factor (α_{tot}) inside the entire magnetosphere *at resonance* (the frequency of EM waves is identical to ω_g).

2. For a given conversion factor, we obtain the Poynting vector of the resultant EM waves along the direction of propagation (S_z). Then, we compare the theoretically derived Poynting vector with the observation of peak flux with the reported FRBs.

To evaluate the conversion factor, solving the linearized covariant Maxwell's equations leads to the following electric and magnetic fields induced due to GWs, i.e., \tilde{E}_x and \tilde{B}_y as:

$$\tilde{E}_x \simeq -\frac{A_+}{2} B_y^{(0)} (1 - \xi \omega_B t) e^{i(k_g z - \omega_g t)} \quad (2)$$

$$\tilde{B}_y \simeq -\frac{A_+}{4} B_y^{(0)} (1 + 2\xi \omega_g t) e^{i(k_g z - \omega_g t)}, \quad (3)$$

where $\xi \equiv \delta B_y / B_y^{(0)}$. Note that the amplitude of \tilde{B}_y has a dependence on ω_g , while the amplitude of \tilde{E}_x has ω_B dependence on ω_g . This is because the induced electric field arises due to the time varying magnetic field. See Eq. (A4) in appendix A.

The conversion factor (α) — ratio of the energy density of EM wave and GWs — gives the efficiency of the process at resonance. α for this process is

$$\alpha \equiv \frac{\rho_{\text{EM}}}{\rho_{\text{GW}}} \simeq \frac{5G|B_y^{(0)}|^2}{8c^2} \left[\frac{4}{5} \xi^2 \left(\frac{z}{c}\right)^2 + \frac{4}{5} \frac{\xi}{\omega_g} \frac{z}{c} + \frac{1}{\omega_g^2} \right] \quad (4)$$

where z refers to the radial distance in the magnetosphere. The details in the appendix. The above expression is the conversion factor at a single point on the magnetosphere. Assuming that there is no cross-correlation of GZ-effect at two distinct points in the magnetosphere, we obtain the total conversion by integrating over the entire magnetosphere (from the surface of the compact object to the light cylinder R_{LC})¹. Thus, the total conversion factor is

$$\alpha_{\text{tot}} \simeq \frac{5\pi G|B_y^{(0)}|^2}{2c^2} \left[\frac{4}{15} \xi^2 \left[\frac{R_{\text{LC}}}{c}\right]^2 + \frac{2\xi R_{\text{LC}}}{5\omega_g c} + \frac{1}{\omega_g^2} \right]. \quad (5)$$

The details are in the appendix. It is important to note that α_{tot} is *independent of the amplitude* of GWs. To understand the variation of α_{tot} with ω_g , in Fig. 2, we have plotted the conversion factor for magnetar and NS/milli-second pulsar.

From the plots, we infer that the total conversion factor is almost insensitive at higher-frequencies (> 1 MHz) for both types of compact objects. This is because the second and

¹ The cross-correlation corresponds to the induced EM waves at two distinct points affecting each other.

This physically corresponds to higher-order effects ($A_+ \partial_z \tilde{B}_y$) which are neglected.

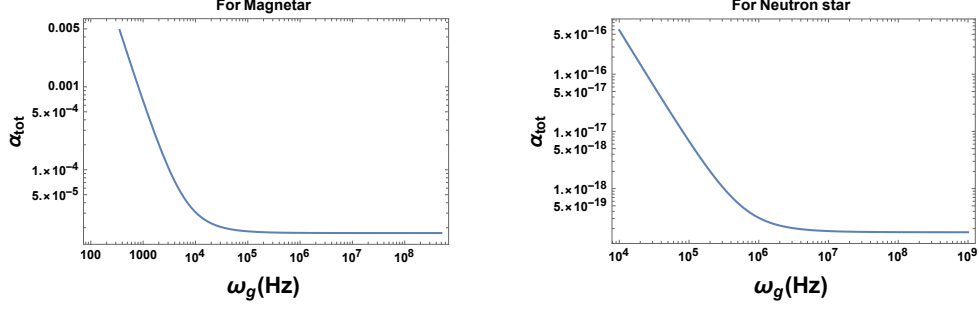


FIG. 2. Log-Log plot of α_{tot} versus ω_g for typical magnetar (left plot) and typical NS (right plot). For magnetar, we set $B_y^{(0)} = 10^{15}$ G, $R_{\text{LC}} = 10^9$ cm, $\omega_B = 1$ Hz. For NS, we set $B_y^{(0)} = 10^{10}$ G, $R_{\text{LC}} = 10^7$ cm, $\omega_B = 1$ kHz.

third terms in RHS of Eq. (5) are inversely proportional to ω_g and, hence, the contribution to α_{tot} is only from the first term. To elaborate, Fig. 3 plots each of these terms in Eq. (5) which shows a clear distinction between milli-second Pulsar and magnetar. In both cases, the cross-over occurs below 1 MHz. Since we are interested in radio frequency in the GHz range, the total conversion factor (5) is independent of the incoming GW frequency.

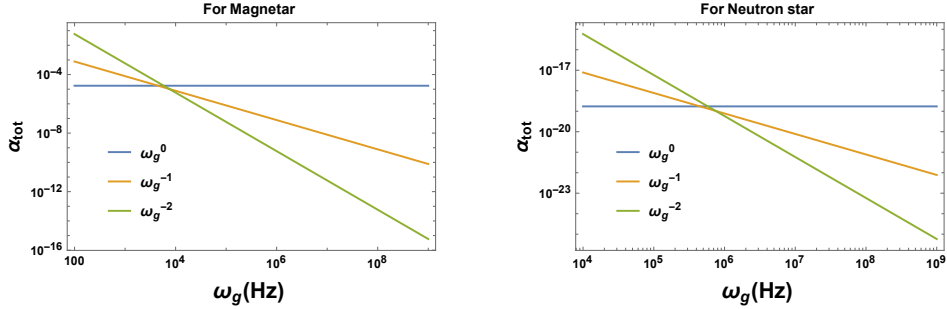


FIG. 3. Log-Log plot of the three terms in the RHS of Eq. (5) versus ω_g for typical magnetar (left plot) and typical NS (right plot). For magnetar, we have set $B_y^{(0)} = 10^{15}$ G, $R_{\text{LC}} = 10^9$ cm, $\omega_B = 1$ Hz. For NS/milli-second pulsar, we have set $B_y^{(0)} = 10^{10}$ G, $R_{\text{LC}} = 10^7$ cm, $\omega_B = 1$ kHz.

This leads to the important question: What is the efficiency of the GZ-effect near magnetar and NS? Table (I) lists the total conversion factor (4th column) for magnetar and NS for different frequencies. We want to emphasize the following points: First, we have assumed that the amplitude of the GWs, i.e., $A_+ = A_\times = 10^{-23}$ corresponding to a typical GW source [18, 20]. However, as we show below, even with this conservative value, the model explains the peak flux of FRBs. Second, α_{tot} is very high near the magnetar for low-frequency

GWs. Specifically, the conversion is 0.06% and 0.25% at 1000 Hz and 500 Hz, respectively (for the magnetar $B_y^{(0)} = 10^{15}$ G). For high-frequency GWs, as we show below, even a total conversion factor (α_{tot}) of 10^{-19} can lead to appreciable energy in the radio frequency (GHz range).

R_{LC} (cm)	$B_y^{(0)}$ (Gauss)	ω_g (MHz)	α_{tot}	ρ_{EM} (Jy cm $^{-1}$ s Hz)	$\frac{S_z}{\omega_g}$ (Jy)
10^9	10^{15}	1	1.74×10^{-5}	4.65×10^{10}	9.95×10^{11}
10^9	10^{12}	500	1.72×10^{-11}	1.15×10^{10}	9.94×10^5
10^8	10^{11}	1400	1.72×10^{-15}	9.07×10^6	961.57
10^7	10^{10}	1400	1.72×10^{-19}	9.07×10^2	0.99
10^8	10^9	1400	1.72×10^{-19}	9.07×10^2	0.09

TABLE I. The table contains numerical values of the total conversion factor (α_{tot}), energy density of EM waves (ρ_{EM}), and spectral flux density (Poynting vector per unit frequency). The first two rows are for a typical Magnetar and the last three rows are for a typical NS. We have set $A_+ = 10^{-23}$ corresponding to a typical GW source [20].

Further, to compare the generated EM energy density in the entire magnetosphere with the observations, we compute the flux of the induced EM waves (2, 3) by calculating the Poynting vector [35]. Rewriting Eq. (5) as a quadratic equation in $\xi R_{\text{LC}}/c$ provides the functional dependence in-terms of α_{tot} . This leads to:

$$S_z \simeq \frac{A_+^2 |B_y^{(0)}|^2 c}{128\pi} \left[\sqrt{\frac{24c^2 \omega_g^2 \alpha_{\text{tot}}}{\pi G |B_y^{(0)}|^2} - 51} - \frac{6c^2 \omega_g \omega_B \alpha_{\text{tot}}}{\pi G |B_y^{(0)}|^2} - 1 \right]. \quad (6)$$

The details are in the appendix. Thus, the Poynting vector of the induced EM waves in the vicinity of magnetar/NS can be obtained by substituting the the parameters of magnetar/NS, ω_g and A_+ . To compare with the peak flux of FRBs, Fig. 4 contains the plot of the Poynting vector per unit frequency (S_z/ω_g) as a function of ω_g for magnetar and NS.

The last column in Table (I) contains the spectral flux density (Poynting vector per unit frequency) for generic parameter ranges of R_{LC} and $B_y^{(0)}$. Given the parameters listed in the table (I), our model predicts a range of spectral flux density that can be as small as 0.1 Jy (milli-second Pulsar) and can be as large as 10^{11} Jy (Magnetar). We are now in a position to compare the results of the model with radio observations in GHz frequency.

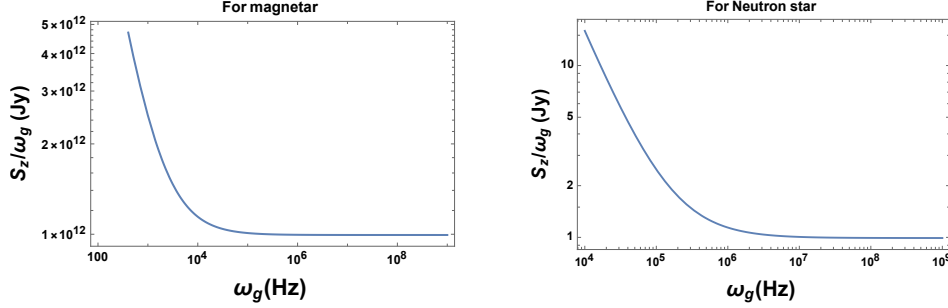


FIG. 4. Log-Log plot of S_z/ω_g versus ω_g for typical magnetar (left plot) and typical NS (right plot). For magnetar, we have set $B_y^{(0)} = 10^{15}$ G, $R_{LC} = 10^9$ cm, $\omega_B = 1$ Hz. For NS/milli-second pulsar, we have set $B_y^{(0)} = 10^{10}$ G, $R_{LC} = 10^7$ cm, $\omega_B = 1$ kHz. For both plots we have set $A_+ = 10^{-23}$ corresponding to a typical GW source [20].

As mentioned earlier, more than 600 FRBs have been reported in various catalogues [5–9]. 99% of these FRBs were found to have the following two characteristic features: peak flux (S_ν) varies in the range $0.1 \text{ Jy} < S_\nu < 700 \text{ Jy}$ and the pulse width is less than one second [6, 9]. As mentioned earlier, R_{LC} of a typical NS is $\sim 10^7 - 10^9$ cm and it takes less than one second for the GWs to pass through the entire magnetosphere. This directly implies that the induced EM waves due to GZ-effect will appear as a burst lasting for less than one second. Thus, our model provides a natural explanation for FRBs lasting for less than a second. Further, we see from the last column of Table (I), our model predicts the burst of EM wave with the flux < 1000 Jy. Thus, our model naturally explains the observed peak flux and pulse width of 99% of the reported FRBs.

Given this, we can now identify the possible progenitors of FRBs. To identify this, we consider two FRBs — FRB120127 [36] and FRB011025 [37]. These two sources represent a typical FRB in the catalogs. The observations of these two FRBs at 1.5 and 1.3 GHz, show a typical peak flux of $0.62^{+0.35}_{-0.10}$ Jy and $0.54^{+0.11}_{-0.07}$ Jy, respectively. From the last row of the Table (I), we see that our model predicts the progenitor should be a millisecond pulsar with an effective magnetic field strength of 10^{10} G and $R_{LC} \sim 10^7$ cm. We can do a similar analysis for all the FRBs in the catalog with a pulse width less than one second [6, 9]. Our model predicts that the progenitor should be a NS with an effective magnetic field strength in the range $10^9 - 10^{11}$ G and rotation frequency $1 < \omega_B < 1000$. Our model naturally explains the observed peak flux for *all reported FRBs* and predicts FRBs with extremely

low and high peak flux. Such future detections will further strengthen the model. Thus, our model is neither sensitive to the galactic environment nor requires exotic new physics to explain FRBs.

Current observations can not accurately localize and provide the distance of these FRBs, leading to uncertainty in the origin of these events. However, our model predicts that the progenitor of these events is a NS in any galaxy. Thus, our model predicts that FRBs can also be extragalactic in origin. Further, our model can explain why certain FRBs are random, and other FRBs repeat at unpredictable intervals. It is known in the literature that GWs in GHz frequency are generated due to plasma instability and/or primordial black holes [16–21]. GWs generated from this or another mechanism passing through the magnetosphere of NS lead to random and repeated FRBs. We thus conclude that the pulsars with the period $1 - 10^{-3}$ s are the progenitor of FRBs. There is a huge international effort with existing telescopes (uGMRT, VLA, ATCA) and upcoming facilities like SKA to search for NS/pulsars outside the Milky Way. The detection of extragalactic milli-second Pulsar will validate our model.

A variety of processes generate GWs in a broad range of frequencies [16–21]. However, it is possible to detect these waves only in a limited range. The proposed model provides an indirect mechanism to detect GWs at high frequencies. Interestingly, our model also provides a way to test modified theories of gravity. In this work, we have focused on GWs in general relativity. Certain modified theories like Chern-Simons gravity lead to birefringence [38] which can explain the polarized nature of FRBs. However, exact rotating solutions in these theories are unknown and require sophisticated numerics. Thus, the high-frequency GWs will provide a unique view of the Universe — it’s birth and evolution.

Acknowledgements The authors thank Sushan Konar and Surjeet Rajendran for discussions. The authors thank Koustav Chandra, S. M. Chandran, Archana Pai, and T. R. Seshadri for their comments on the earlier draft. AK thanks L. F. Wei for clarifications in Ref. [36]. AK is supported by the MHRD fellowship at IIT Bombay. This work is supported by ISRO Respond grant.

Appendix A: Gertsenshtein-Zel’dovich effect and induced electromagnetic waves

Consider a background space-time with gravitational waves (GWs) [33]:

$$g_{\alpha\beta} = \eta_{\alpha\beta} + h_{\alpha\beta} = \begin{pmatrix} 1 & 0 & 0 & 0 \\ 0 & -1 + h_+ & h_\times & 0 \\ 0 & h_\times & -1 - h_+ & 0 \\ 0 & 0 & 0 & -1 \end{pmatrix}, \quad (\text{A1})$$

where $h_{\alpha\beta} \ll 1$ is the GWs fluctuation, and $\eta_{\alpha\beta} = \text{diag}(1, -1, -1, -1)$ is Minkowski space-time. The inverse of the metric can be obtained as $g^{\alpha\beta} = \eta^{\alpha\beta} - h^{\alpha\beta}$ up to linear order. The background space-time is generally curved; however, the results derived for Minkowski space-time carry through the conversion factor computations. For the generic curved background, the Riemann corrections contribution is very tiny [33]. Hence, we only report the results about the Minkowski space-time.

Since the equations are linear, we consider a monochromatic circularly polarized GWave propagating along the z-direction. Thus, rewriting the circularly polarized wave in-terms of the h_+ and h_\times in Eq. (A1) leads to [26, 33]:

$$h_+ = h_{xx} = -h_{yy} = A_+ e^{i(k_g z - \omega_g t)}, \quad h_\times = h_{xy} = h_{yx} = iA_\times e^{i(k_g z - \omega_g t)}, \quad (\text{A2})$$

where k_g and ω_g refer to the wave vector and frequency of the GWs, A_+ and A_\times are the amplitude of the GWs which are constant in space and time. As mentioned earlier, the presence of magnetic field transverse to the direction of propagation of GWs acts as a catalyst for the conversion process [24–27]. As discussed in the main text, we consider the total magnetic field in the magnetosphere to be [26]

$$\mathbf{B}(t) = (0, B_y^{(0)} + \delta B_y \sin(\omega_B t), 0) \quad (\text{A3})$$

where $B_y^{(0)}$ is static magnetic field and $\delta B_y \sin(\omega_B t)$ is the alternating (time-varying) magnetic field with frequency $1 < \omega_B (\text{s}^{-1}) < 10^3$ and $|\delta B_y| < |B_y^{(0)}|$. Also, we assume that the amplitude of the alternating magnetic field is two orders lower than the static magnetic field, i.e., $\left| \frac{\delta B_y}{B_y^{(0)}} \right| \approx 10^{-2}$, so that time-varying magnetic field has significant effects on the conversion [31, 32]

The induced electric field due to the time-varying magnetic field is given by [39]

$$\mathbf{E}(z, t) = \left(-\frac{z \omega_B \delta B_y}{c} \cos(\omega_B t), 0, 0 \right). \quad (\text{A4})$$

In the absence of GWs, the non-zero components of the background electromagnetic (EM) field tensor $F_{\alpha\beta}^{(0)}$ is:

$$F_{01}^{(0)} = E_x = -F_{10}^{(0)} = -\frac{z \delta B_y \omega_B}{c} \cos(\omega_B t); \quad F_{13}^{(0)} = B_z = -F_{31}^{(0)} = B_y^{(0)} + \delta B_y \sin(\omega_B t). \quad (\text{A5})$$

In the presence of GWs, the EM field tensor can be represented as:

$$F_{\alpha\beta} = F_{\alpha\beta}^{(0)} + F_{\alpha\beta}^{(1)} = \begin{pmatrix} 0 & \mathcal{E}_x & \tilde{E}_y & \tilde{E}_z \\ -\mathcal{E}_x & 0 & -\tilde{B}_z & \mathcal{B}_y \\ -\tilde{E}_y & \tilde{B}_z & 0 & -\tilde{B}_x \\ -\tilde{E}_z & -\mathcal{B}_y & \tilde{B}_x & 0 \end{pmatrix}, \quad (\text{A6})$$

where $F_{\alpha\beta}^{(1)}$ is the field tensor induced due to the GWs that needs to be determined. Similarly, the induced electric $[\tilde{\mathbf{E}} = (\tilde{E}_x, \tilde{E}_y, \tilde{E}_z)]$ and magnetic field vectors $[\tilde{\mathbf{B}} = (\tilde{B}_x, \tilde{B}_y, \tilde{B}_z)]$ due to GWs are to be determined. Note that $\mathcal{B}_y = B_y^{(0)} + \delta B_y \sin(\omega_B t) + \tilde{B}_y$ and $\mathcal{E}_x = -\frac{z \delta B_y \omega_B}{c} \cos(\omega_B t) + \tilde{E}_x$. The covariant Maxwell's equations (in the source-free region) are:

$$\partial_\mu (\sqrt{-g} F^{\mu\nu}) = \partial_\mu (\sqrt{-g} g^{\mu\alpha} g^{\nu\beta} F_{\alpha\beta}) = 0 \quad (\text{A7a})$$

$$\partial_\mu (\sqrt{-g} \tilde{F}^{\mu\nu}) = \partial_\mu (\sqrt{-g} \eta^{\mu\nu\alpha\beta} F_{\alpha\beta}) = 0 \quad (\text{A7b})$$

where $\tilde{F}^{\mu\nu} = \epsilon^{\mu\nu\alpha\beta} F_{\alpha\beta}/2$ is the dual of EM field tensor, $\epsilon^{\mu\nu\alpha\beta} = \eta^{\mu\nu\alpha\beta}/\sqrt{-g}$ and $\eta^{\mu\nu\alpha\beta}$ is defined as $\eta^{0123} = 1 = -\eta_{0123}$ is an antisymmetric tensor. Substituting Eq. (A6) in (A7a, A7b), and treating $F_{\alpha\beta}^{(1)}$ and $h_{\alpha\beta}$ as first-order perturbations, we have

$$\partial_\mu \left[(\eta^{\mu\alpha} h^{\nu\beta} + h^{\mu\alpha} \eta^{\nu\beta}) F_{\alpha\beta}^{(0)} - \eta^{\mu\alpha} \eta^{\nu\beta} F_{\alpha\beta}^{(1)} \right] = 0 \quad (\text{A8a})$$

$$\partial_\mu \left(\eta^{\mu\nu\alpha\beta} F_{\alpha\beta}^{(1)} \right) = 0. \quad (\text{A8b})$$

For the metric corresponding to the two-modes of polarization of GWs (A1), the two Maxwell's equations (A8a, A8b), in terms of electric and magnetic fields are given by:

$$\frac{1}{c} \partial_t \tilde{E}_x - \partial_y \tilde{B}_z + \partial_z \tilde{B}_y + (B^{(0)} + \delta B_y \sin(\omega_B t)) \partial_z h_+ - \frac{z \delta B_y \omega_B}{c^2} \frac{\partial}{\partial t} (h_+ \cos(\omega_B t)) = 0 \quad (\text{A9a})$$

$$\frac{1}{c} \partial_t \tilde{B}_y - \partial_x \tilde{E}_z + \partial_z \tilde{E}_x = 0. \quad (\text{A9b})$$

The above two equations lead to the following wave equations:

$$\begin{aligned} \frac{1}{c^2} \frac{\partial^2 \tilde{E}_x}{\partial t^2} - \partial_z^2 \tilde{E}_x &= -\frac{\delta B_y \omega_B}{c} \cos(\omega_B t) \partial_z h_+ - \frac{1}{c} (B^{(0)} + \delta B_y \sin(\omega_B t)) \partial_t \partial_z h_+ \\ &+ \frac{z \delta B_y \omega_B}{c^3} \frac{\partial^2}{\partial t^2} (h_+ \cos(\omega_B t)) \end{aligned} \quad (\text{A10a})$$

$$\begin{aligned} \frac{1}{c^2} \frac{\partial^2 \tilde{B}_y}{\partial t^2} - \partial_z^2 \tilde{B}_y &= (B^{(0)} + \delta B_y \sin(\omega_B t)) \partial_z^2 h_+ - \frac{\delta B_y \omega_B}{c^2} \partial_t (h_+ \cos(\omega_B t)) \\ &- \frac{z \delta B_y \omega_B}{c^2} \partial_t \partial_z (h_+ \cos(\omega_B t)) \end{aligned} \quad (\text{A10b})$$

Since GWs (and EM waves) propagate along the z -direction, we have $\tilde{E}_z = \tilde{B}_z = 0$. Substituting Eq. (A2) in Eqns. (A10a) and (A10b) in the above wave equations lead to the following wave equations for \tilde{E}_x, \tilde{B}_y :

$$\frac{1}{c^2} \frac{\partial^2 \tilde{E}_x}{\partial t^2} - \partial_z^2 \tilde{E}_x = f_E(z', t') \quad (\text{A11a})$$

$$\frac{1}{c^2} \frac{\partial^2 \tilde{B}_y}{\partial t^2} - \partial_z^2 \tilde{B}_y = f_B(z', t') \quad (\text{A11b})$$

where $f_{E/B}(z', t')$ are the forcing functions and are given by:

$$\begin{aligned} f_E(z', t') &= -\frac{A_+ B^{(0)} k_g \omega_g}{c} e^{i(k_g z' - \omega_g t')} - \frac{i A_+ \delta B_y k_g}{2c} \left(\omega_+ e^{i(k_g z' - \omega_+ t')} - \omega_- e^{i(k_g z' - \omega_- t')} \right) \\ &- \frac{z' A_+ \delta B_y \omega_B}{2c^3} \left(\omega_+^2 e^{i(k_g z' - \omega_+ t')} + \omega_-^2 e^{i(k_g z' - \omega_- t')} \right) \end{aligned} \quad (\text{A12a})$$

$$\begin{aligned} f_B(z', t') &= -A_+ B^{(0)} k_g^2 e^{i(k_g z' - \omega_g t')} - \frac{i A_+ \delta B_y k_g^2}{2} \left(e^{i(k_g z' - \omega_+ t')} - e^{i(k_g z' - \omega_- t')} \right) \\ &- \frac{i A_+ \delta B_y \omega_B}{2c^2} \left(\omega_+ e^{i(k_g z' - \omega_+ t')} - \omega_- e^{i(k_g z' - \omega_- t')} \right) \\ &+ \frac{z' A_+ \delta B_y \omega_B k_g}{2c^2} \left(\omega_+ e^{i(k_g z' - \omega_+ t')} - \omega_- e^{i(k_g z' - \omega_- t')} \right) \end{aligned} \quad (\text{A12b})$$

and $\omega_{\pm} = \omega_g \pm \omega_B$. The solutions to the wave equations (A11a) and (A11b) are given by:

$$F_{E/B}(z, t) = \int \int dz' dt' G(t, t'; z, z') f_{E/B}(t', z') \quad (\text{A13})$$

where $F_{E/B}(z, t)$ denotes the corresponding solution of the forcing function $f_{E/B}(z', t')$ and $G(t, t'; z, z')$ is the retarded Green's function corresponding to the wave equation and is given by:

$$G(t, t'; z, z') = \frac{c}{2} \Theta (c(t - t') - |z - z'|) \quad (\text{A14})$$

where Θ -function is non-zero only for $t \geq t' + \frac{|z-z'|}{c}$. Substituting the forcing functions for the electric (A12a) and the magnetic (A12b) fields, in the integral equation (A13), leads to:

$$\tilde{E}_x \simeq -\frac{B_y^{(0)} A_+}{2} e^{i(k_g z - \omega_g t)} + \frac{\delta B_y A_+ \omega_B t}{2} e^{i(k_g z - \omega_g t)} + \frac{\delta B_y A_+}{4i} \left(\frac{\omega_B}{\omega_g}\right) e^{i(k_g z - \omega_g t)} \quad (\text{A15})$$

$$\tilde{B}_y \simeq -\frac{B_y^{(0)} A_+}{4} e^{i(k_g z - \omega_g t)} - \frac{\delta B_y A_+ \omega_g t}{2} e^{i(k_g z - \omega_g t)} + \frac{\delta B_y A_+}{4i} \left(\frac{\omega_B}{\omega_g}\right)^2 e^{i(k_g z - \omega_g t)}. \quad (\text{A16})$$

We want to mention the following points regarding the above expressions: First, in obtaining the above expressions, we have assumed that $\omega_B \ll \omega_g$. This is valid in our case because the conversion from GWs to EM waves occurs in the sub-GHz frequency range. This approximation leads to $\omega_{\pm}^n \simeq \omega_g^n \left(1 \pm n \frac{\omega_B}{\omega_g}\right)$ and allows us to approximate $\omega_{\pm} \approx \omega_g$ in the exponentials. Note that we have also ignored the terms with $e^{i\omega_g t}$ since they will lead to wave propagating along negative z-direction i.e., $e^{i(k_g z + \omega_g t)}$, and hence are not relevant to our analysis. Second, the last term in both the expressions is tiny and can be neglected. Thus, we have

$$\tilde{E}_x \simeq -\frac{B_y^{(0)} A_+}{2} e^{i(k_g z - \omega_g t)} + \frac{\delta B_y A_+ \omega_B t}{2} e^{i(k_g z - \omega_g t)} \quad (\text{A17})$$

$$\tilde{B}_y \simeq -\frac{B_y^{(0)} A_+}{4} e^{i(k_g z - \omega_g t)} - \frac{\delta B_y A_+ \omega_g t}{2} e^{i(k_g z - \omega_g t)} \quad (\text{A18})$$

In the next section, we will use the above expressions to obtain the conversion factor for the entire magnetosphere.

Appendix B: Conversion factor from entire magnetosphere

In this section, we will estimate the total conversion factor from the entire magnetosphere of the compact object. We also show that the assumption that the background magnetic field can be treated as a constant in the entire magnetosphere gives identical results to that of the background field decreasing radially.

1. Conversion factor calculation

The energy density carried by these induced EM waves is [39]

$$\rho_{\text{EM}} = \frac{|\tilde{E}_x|^2 + |\tilde{B}_y|^2}{8\pi} \simeq \frac{|A_+|^2 |B_y^{(0)}|^2}{16 \times 8\pi} [5 + 4\xi^2 \omega_g^2 t^2 + 4\xi \omega_g t]. \quad (\text{B1})$$

where $\xi = \delta B_y / B_y^{(0)}$. As mentioned earlier, the conversion is maximum when EM waves are approximately the same as the incoming waves. Having obtained the energy carried by the induced EM waves, we need to obtain what fraction of wave energy is converted to EM waves [25]? To do this, we calculate the energy density carried by the GWs [33], i. e.:

$$\rho_{\text{GW}} = \frac{c^2 \omega_g^2}{32\pi G} (|A_+|^2 + |A_\times|^2) = \frac{c^2 \omega_g^2}{16\pi G} |A_+|^2, \quad (\text{B2})$$

wherein second equality, we have used the fact that both the modes of GWs are generated with an equal amount of energy, i.e., $|A_+| = |A_\times|$ also referred to as isospectrality relation [34].

From Eqs. (B1, B2), we obtain the following conversion factor (α):

$$\alpha \equiv \frac{\rho_{\text{EM}}}{\rho_{\text{GW}}} \simeq \frac{5G|B_y^{(0)}|^2}{8c^2} \left(\frac{4}{5} \xi^2 \left(\frac{z}{c} \right)^2 + \frac{4}{5} \frac{\xi}{\omega_g} \frac{z}{c} + \frac{1}{\omega_g^2} \right), \quad (\text{B3})$$

where we have substituted $t = z/c$ and z is the distance traveled by the wave.

To obtain the conversion factor in the entire magnetosphere, we define the following dimensionless parameter:

$$X = \frac{r}{R_{\text{LC}}} \quad (\text{B4})$$

where r is the distance from the surface of neutron star to a point in the magnetosphere, i.e., $r_* \lesssim r \lesssim R_{\text{LC}}$, and $r_*(= 10^6 \text{ cm})$ is the radius of the Neutron star (NS). In the case of Magnetar $R_{\text{LC}} = 10^9 \text{ cm}$ and for NS $R_{\text{LC}} = 10^7 \text{ cm}$, hence, $X_* = \frac{r_*}{R_{\text{LC}}} < 1$. In other words, the range of X is $0.001 \lesssim X \lesssim 1$.

Since we are interested in the EM waves reaching the observer, we are interested in evaluating the conversion factor along the observer's line of sight. Thus, we have

$$z = r = X R_{\text{LC}}. \quad (\text{B5})$$

where $\theta = 0$ corresponds to the direction along the line-of-sight of the observer. Thus, the total conversion factor is given by the integral

$$\alpha_{\text{tot}} = \Omega \int_{X_*}^1 \alpha dX, \quad (\text{B6})$$

where Ω is the total solid angle which is an overall constant factor because Eq.(B3) is independent of the angular coordinates.

2. Evaluating the radius of the magnetosphere

In evaluating α_{tot} , we have assumed that the background magnetic field is a constant until light cylinder radius R_{LC} . In this section, we show that this assumption is physically consistent.

To do that, we consider the magnetic field of the pulsar magnetosphere in vacuum to be dipolar. We evaluate the average dipolar magnetic field in the magnetosphere. In spherical polar coordinates, the dipolar magnetic field is given by [40, 41]:

$$(B_r, B_\theta, B_\phi) = B_* \left(\frac{r_*}{r}\right)^3 (2 \cos \theta, \sin \theta, 0) \quad (\text{B7})$$

where B_* is the magnetic field on the NS surface.

We now compute the average magnetic field on the volume between the radius of the NS (r_*) and R_{LC} :

$$\bar{\mathbf{B}}(r, \theta, \phi) = \frac{1}{V} \int_{r_*}^{R_{\text{LC}}} dr \int_0^\pi d\theta \int_0^{2\pi} d\phi r^2 \sin \theta \mathbf{B}(r, \theta, \phi) \quad (\text{B8})$$

where V is the volume enclosed by both the surfaces and is given by

$$V = \int_{r_*}^{R_{\text{LC}}} dr \int_0^\pi d\theta \int_0^{2\pi} d\phi r^2 \sin \theta = \frac{4\pi}{3} (R_{\text{LC}}^3 - r_*^3). \quad (\text{B9})$$

From Eqs. (B8, B9), we define the integral \mathcal{I} as:

$$\mathcal{I} \equiv V \bar{\mathbf{B}}(r, \theta, \phi) = \int_{r_*}^{R_{\text{LC}}} dr \int_0^\pi d\theta \int_0^{2\pi} d\phi r^2 \sin \theta \mathbf{B}(r, \theta, \phi). \quad (\text{B10})$$

Note that the volume average of the radial component of the magnetic field vanishes.

$$\bar{\mathbf{B}}_r = \frac{1}{V} \int_{r_*}^{R_{\text{LC}}} dr \int_0^\pi d\theta \int_0^{2\pi} d\phi \left(2B_* \left(\frac{r_*}{r}\right)^3 r^2 \sin \theta \cos \theta \right) = 0. \quad (\text{B11})$$

The only non-zero contribution comes from the angular variation of the magnetic field, i.e.,

$$\bar{\mathbf{B}}_\theta = \frac{1}{V} \int_{r_*}^{R_{\text{LC}}} dr \int_0^\pi d\theta \int_0^{2\pi} d\phi \left(B_* \left(\frac{r_*}{r}\right)^3 r^2 \sin^2 \theta \right) = \frac{3\pi B_* r_*^3}{4(R_{\text{LC}}^3 - r_*^3)} \ln \left| \frac{R_{\text{LC}}}{r_*} \right|. \quad (\text{B12})$$

From Eqs. (B10, B12), we obtain

$$\mathcal{I} = \int_{r_*}^{R_{\text{LC}}} dr \int_0^\pi d\theta \int_0^{2\pi} d\phi r^2 \sin \theta \mathbf{B}(r, \theta, \phi) = \pi^2 B_* r_*^3 \ln \left| \frac{R_{\text{LC}}}{r_*} \right| \quad (\text{B13})$$

We now compare this with the assumption that the magnetic field is approximately constant until R_{LC} . To do this, we substitute the average magnetic field obtained in Eq. (B12) inside the integral in Eq.(B10). Doing the radial integral between r_* to \mathcal{R} leads to:

$$\mathcal{I} = \int_{r_*}^{\mathcal{R}} dr \int_0^\pi d\theta \int_0^{2\pi} d\phi r^2 \sin\theta \bar{B}_\theta = \pi^2 B_* r_*^3 \frac{(\mathcal{R}^3 - r_*^3)}{(R_{\text{LC}}^3 - r_*^3)} \ln \left| \frac{R_{\text{LC}}}{r_*} \right|. \quad (\text{B14})$$

Setting $\mathcal{R} = R_{\text{LC}}$ in the above expression, we see that the two expressions (B13, B14) are approximately the same. Thus, even if there is a radial and angular variation in the magnetic field in the magnetosphere, we can approximate the background field to be approximately constant in the region $r_* \leq r \leq R_{\text{LC}}$. Thus, our expression for the total conversion factor mimics the realistic NS regions.

Appendix C: Poynting vector of the resultant EM waves

In astrophysical observations of compact objects, a quantity of interest is the energy flux density which is the Poynting vector. This section evaluates the Poynting vector for magnetar and neutron star in CGS unit and Jansky Hz, a widely used unit for flux density in radio observations.

The Poynting vector of the induced electric field (A17) and induced magnetic field (A18) is [39]:

$$S_z = \frac{c}{8\pi} \tilde{E}_x \times \tilde{B}_y^* \simeq \frac{A_+^2 |B_y^{(0)}|^2 c}{64\pi} \left[1 + 2\omega_g \xi \frac{R_{\text{LC}}}{c} - 2\omega_g \omega_B \xi^2 \left(\frac{R_{\text{LC}}}{c} \right)^2 \right] \quad (\text{C1})$$

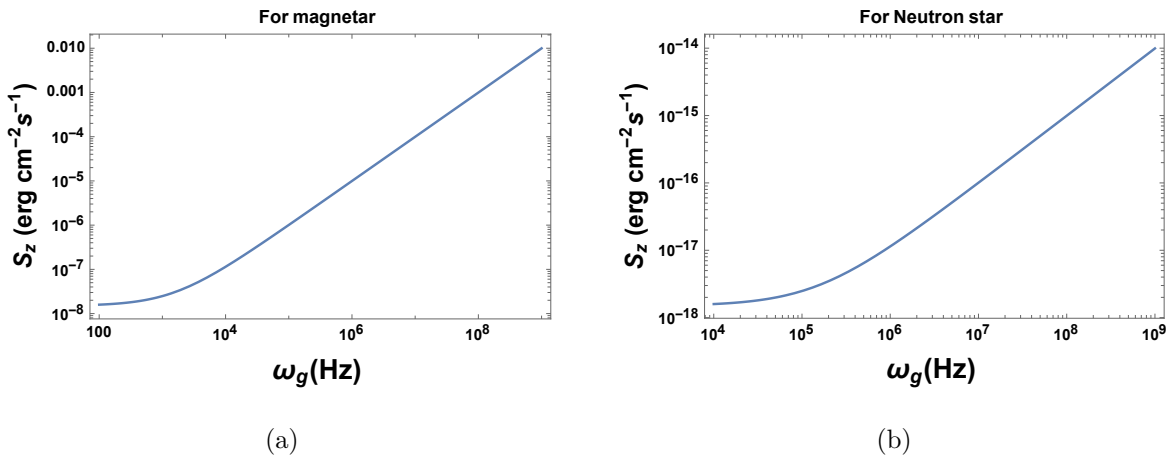


FIG. 5. Log-log Plots of S_z versus ω_g for magnetar (left) and NS (right plot).

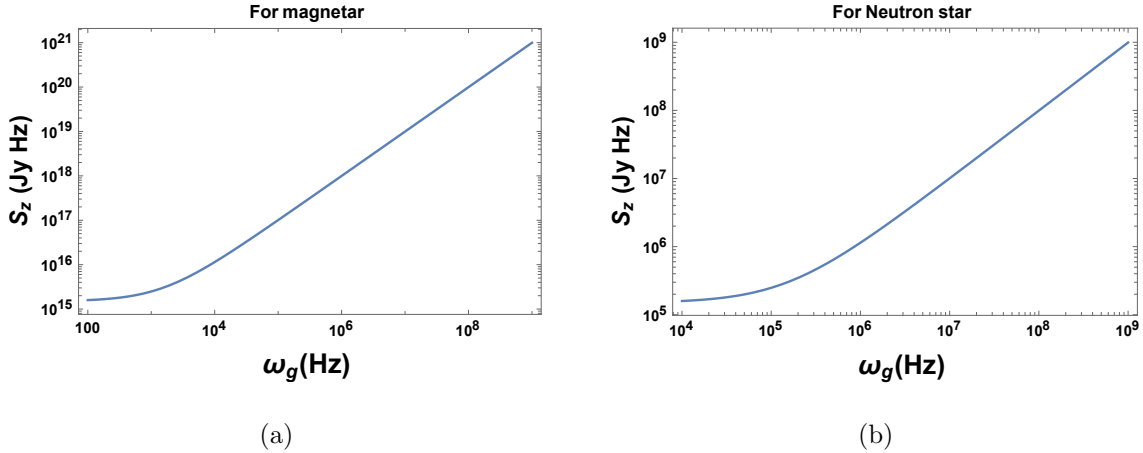


FIG. 6. Log-log Plots of S_z versus ω_g for magnetar (left) and NS (right plot).

where \tilde{B}_y^* is the complex conjugate of the induced magnetic field \tilde{B}_y . In Fig. 5, we have plotted the Poynting vector (C2) as a function of the frequency of EM waves. As mentioned in the main text, the frequency of the alternating magnetic field is 1Hz for magnetar and 10^3 Hz for the millisecond pulsar.

Rewriting the above Poynting vector in terms of α_{tot} , we have:

$$S_z \simeq \frac{A_+^2 |B_y^{(0)}|^2 c}{128\pi} \left[\left(\frac{24 c^2 \omega_g^2 \alpha_{\text{tot}}}{\pi G |B_y^{(0)}|^2} - 51 \right)^{1/2} - \frac{6 c^2 \omega_g \omega_B \alpha_{\text{tot}}}{\pi G |B_y^{(0)}|^2} - 1 \right]. \quad (\text{C2})$$

Note that α_{tot} in RHS of the above expression is a function of ω_g and the parameters of magnetar/NS. In Fig. 6 we have plotted the Poynting vector (C2) in Jy Hz units.

In these plots, we have set $G = 6.67 \times 10^{-8} \text{dyne cm}^2 \text{gm}^{-2}$, $c = 3 \times 10^{10} \text{cm s}^{-1}$, $A_+ = 10^{-23}$ corresponding to primordial black holes [20]. For Magnetar, we have assumed $B_y^{(0)} = 10^{15} \text{G}$, $R_{\text{Lc}} = 10^9 \text{cm}$, $\omega_B = 1 \text{Hz}$. For milli-second pulsar, we have set $B_y^{(0)} = 10^{10} \text{G}$, $R_{\text{Lc}} = 10^7 \text{cm}$, $\omega_B = 1 \text{kHz}$ [4, 29, 30, 42]. We have used the following unit-conversion factor from CGS unit [erg cm^{-3}] to Jansky (Jy) is $1 \text{erg cm}^{-3} = 10^{23} \text{Jy cm}^{-1} \text{s Hz}$.

-
- [1] D. B. Melrose, M. Z. Rafat, and A. Mastrano, *mnras* **500**, 4530 (2021), [arXiv:2006.15243 \[astro-ph.HE\]](#).
- [2] A. Levan, P. Crowther, R. de Grijs, N. Langer, D. Xu, and S.-C. Yoon, *Space Sci. Rev.* **202**, 33 (2016), [arXiv:1611.03091 \[astro-ph.HE\]](#).
- [3] D. R. Lorimer, *Living Rev. Rel.* **11**, 8 (2008), [arXiv:0811.0762 \[astro-ph\]](#).

- [4] J. M. Cordes and S. Chatterjee, *Ann. Rev. Astron. Astrophys.* **57**, 417 (2019), [arXiv:1906.05878 \[astro-ph.HE\]](#).
- [5] E. Platts, A. Weltman, A. Walters, S. P. Tendulkar, J. E. B. Gordin, and S. Kandhai, *Phys. Rept.* **821**, 1 (2019), [arXiv:1810.05836 \[astro-ph.HE\]](#).
- [6] E. Petroff and et al, *Publ. Astron. Soc. Austral.* **33**, e045 (2016), [arXiv:1601.03547 \[astro-ph.HE\]](#).
- [7] I. Pastor-Marazuela *et al.*, *Nature* **596**, 505 (2021).
- [8] M. Rafei-Ravandi *et al.*, *Astrophys. J.* **922**, 42 (2021).
- [9] M. Rafei-Ravandi *et al.*, *Astrophys. J.* **922**, 42 (2021).
- [10] D. R. Lorimer and M. Kramer, *Handbook of Pulsar Astronomy*, Vol. 4 (2004).
- [11] J. P. Conlon and C. A. R. Herdeiro, *Phys. Lett. B* **780**, 169 (2018), [arXiv:1701.02034 \[astro-ph.HE\]](#).
- [12] M. J. REES, *Nature* **266**, 333 (1977).
- [13] B. Carr and F. Kuhnel, *Annual Review of Nuclear and Particle Science* **70**, 355 (2020).
- [14] T. Vachaspati, *Phys. Rev. Lett.* **101**, 141301 (2008).
- [15] Z. Shand, A. Ouyed, N. Koning, and R. Ouyed, *Res. Astron. Astrophys.* **16**, 080 (2016), [arXiv:1505.08147 \[astro-ph.HE\]](#).
- [16] B. J. Carr and S. W. Hawking, *Mon. Not. Roy. Astron. Soc.* **168**, 399 (1974).
- [17] R. Anantua, R. Easther, and J. T. Giblin, *Phys. Rev. Lett.* **103**, 111303 (2009).
- [18] K. Kuroda, W.-T. Ni, and W.-P. Pan, *Int. J. Mod. Phys. D* **24**, 1530031 (2015), [arXiv:1511.00231 \[gr-qc\]](#).
- [19] A. Ejlli, D. Ejlli, A. M. Cruise, G. Pisano, and H. Grote, *Eur. Phys. J. C* **79**, 1032 (2019), [arXiv:1908.00232 \[gr-qc\]](#).
- [20] N. Aggarwal *et al.*, (2020), [arXiv:2011.12414 \[gr-qc\]](#).
- [21] V. Pustovoit, V. Gladyshev, V. Kauts, A. Morozov, P. Nikolaev, I. Fomin, E. Sharandin, and A. Kayutenko, *J. of Phys: Conf. Ser.* **2081**, 012009 (2021).
- [22] B. S. Sathyaprakash and B. F. Schutz, *Living Rev. Rel.* **12**, 2 (2009), [arXiv:0903.0338 \[gr-qc\]](#).
- [23] B. Schutz, “Gravitational Radiation,” in *Encyclopedia of Astronomy and Astrophysics*, edited by P. Murdin (2000) p. 2110.
- [24] M. E. Gertsenshtein, *Soviet Journal of Experimental and Theoretical Physics* **14** (1962).
- [25] Y. B. Zel’dovich, *Soviet Journal of Experimental and Theoretical Physics* **38**, 652 (1974).

- [26] H. Zheng, L. F. Wei, H. Wen, and F. Y. Li, *Phys. Rev. D* **98**, 064028 (2018).
- [27] V. Domcke and C. Garcia-Cely, *Phys. Rev. Lett.* **126**, 021104 (2021).
- [28] B. C. Andersen *et al.* (CHIME/FRB), *Nature* **587**, 54 (2020), arXiv:2005.10324 [astro-ph.HE].
- [29] R. Belvedere, J. A. Rueda, and R. Ruffini, *Astrophys. J.* **799**, 23 (2015), arXiv:1411.2621 [astro-ph.SR].
- [30] G. I. Melikidze and J. Gil, *Proceedings of the International Astronomical Union* **4**, 131–132 (2008).
- [31] J. A. Pons and D. Viganò, *Living Reviews in Computational Astrophysics* **5**, 3 (2019).
- [32] Pons, J. A., Viganò, D., and Geppert, U., *A&A* **547**, A9 (2012).
- [33] C. W. Misner, K. S. Thorne, and J. A. Wheeler, *Gravitation* (W. H. Freeman, San Francisco, 1973).
- [34] S. Chandrasekhar, *The Mathematical Theory of Black Holes*, International series of monographs on physics (Clarendon Press, 1998).
- [35] G. Rybicki and A. Lightman, *Radiative Processes in Astrophysics* (Wiley, 1979).
- [36] D. Thornton *et al.*, *Science* **341**, 53 (2013), arXiv:1307.1628 [astro-ph.HE].
- [37] S. Burke-Spolaor and K. W. Bannister, *Astrophys. J.* **792**, 19 (2014), arXiv:1407.0400 [astro-ph.HE].
- [38] S. H. S. Alexander, M. E. Peskin, and M. M. Sheikh-Jabbari, *Phys. Rev. Lett.* **96**, 081301 (2006).
- [39] J. D. Jackson, *Classical Electrodynamics* (Wiley, 1998).
- [40] B. Cerutti and A. Beloborodov, *Space Sci. Rev.* **207**, 111 (2017), arXiv:1611.04331 [astro-ph.HE].
- [41] J. Pétri, *J. Plasma Phys.* **82**, 635820502 (2016), arXiv:1608.04895 [astro-ph.HE].
- [42] C. J. White, A. Burrows, M. S. B. Coleman, and D. Vartanyan, (2021), arXiv:2111.01814 [astro-ph.HE].